

## 7. Design of a Muon Accelerator for the Neutrino Factory

### 7.1 Introduction

The muon accelerator must deliver a pulsed 50 GeV beam to the storage ring with an intensity of  $6 \times 10^{20}$  charged particles per year delivered in  $2 \times 10^7$  seconds, an average beam power of 240 kW. Large transverse and longitudinal acceptances are required, and they drive the design toward low rf frequency, especially in the early stages of acceleration. This is reflected in the layout (for example Figure 1 in the introduction), in which the second recirculating linac (RLA2) is seen to be the dominant subsystem of the whole facility. High accelerating gradients are necessary to preserve the muon flux given the short muon lifetime. Were normal-conducting cavities used, achieving high gradients would require high peak power, higher than is available in low-frequency rf sources. The number of sources would be large and the installation would become prohibitively expensive. Superconducting rf (srf) cavities are a much more attractive solution. SRF offers additional advantages: rf power can be delivered to the cavities over an extended time, and power dissipation is of much less concern given the very high cavity quality factor (Q). The muon accelerator is therefore baselined on srf technology.

The accelerator will capture 190 MeV muons from the cooling channel and accelerate them to 50 GeV. Table 1 lists the input parameters, and Table 2 presents derived machine parameters (such as average and peak currents) used in subsequent discussion.

PARAMETER	BASELINE VALUE
$P_{\text{injection}}$	190 MeV/c
$E_{\text{final}}$	50 GeV
$\epsilon_N^{\text{injected}}$	1.5 mm-rad
$\epsilon_N^{\text{extracted}}$	3.2 mm-rad
$\Delta E/E_{\text{final}}$	$< \pm 2\%$
$\sigma_l^{\text{bunch, injected}}$	12 cm
$\sigma_{\delta p/p}^{\text{bunch, injected}}$	11%
macropulse length	four 150 nsec pulses with 250 nsec pulse-to-pulse separation
$N_{\text{bunch}}/\text{macropulse}$	$30 \times 4 = 120$
$N_{\mu}/\text{macropulse, extracted}$	$(1.5 \times \text{design}) 3 \times 10^{12}$
$f_{\text{macropulse}}$	15 Hz

**Table 1:** System Parameters

Parameter	Derived Value	Comments
$I_{\text{ave}}$	7.2 $\mu\text{A}$	Macroscopic average current
$I_{\text{in pulse}}$	0.8 A	Current in quarter-macropulse
$P_{\text{ave}} (1.5 \times \text{design})$	360 kW	Macroscopic average beam power
$P_{\text{in pulse}}$	40 GW	Beam power in quarter-macropulse
$\beta_{\text{injection}} = v/c$	0.87	
$\epsilon_{\text{injected}}^{\text{geometric}} = \epsilon_N^{\text{injected}} / \beta\gamma$	$9 \times 10^{-4}$ m-rad	Injected geometric emittance
$\epsilon_{\text{extracted}}^{\text{geometric}} = \epsilon_N^{\text{extracted}} / \beta\gamma$	$6.4 \times 10^{-6}$ m-rad	Extracted geometric emittance
$\sigma_{\text{betatron}}^{\text{injected}} (\beta = 1 \text{ m})$	3 cm	Injected rms spot size at beam envelope of 1 m
$\sigma_{\text{betatron}}^{\text{extracted}} (\beta = 10 \text{ m})$	8 mm	Extracted rms spot size at beam envelope of 10 m

**Table 2:** Derived Parameters

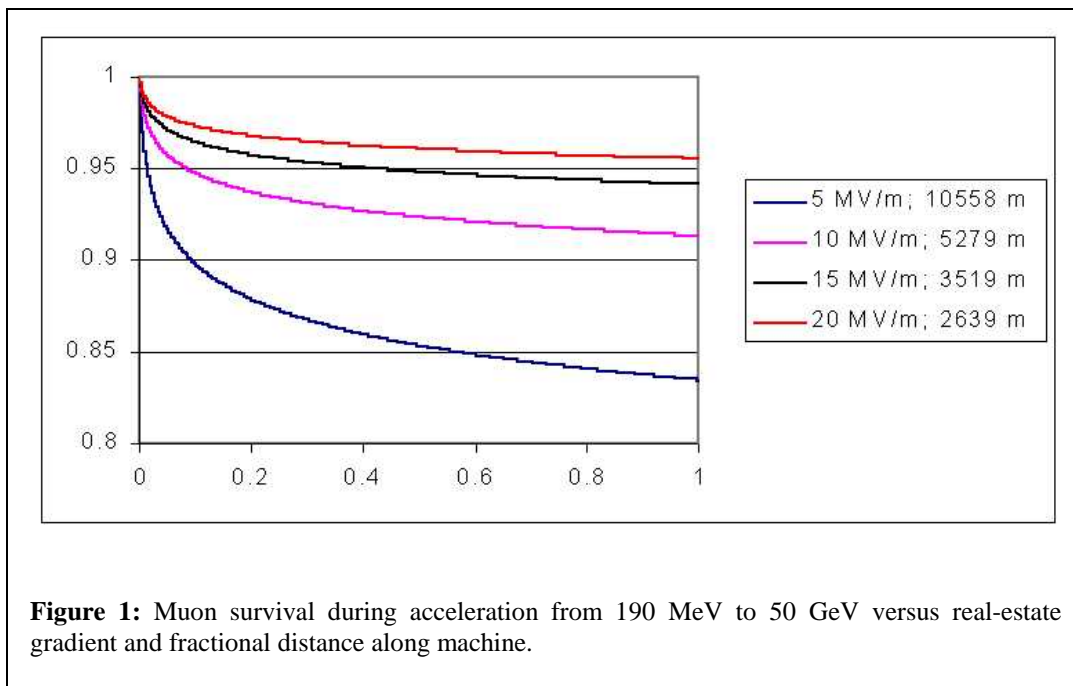
### 7.2 Fundamental Issues

The primary technical issues, to be discussed in this chapter, are:

- muon survival,
- choice of accelerating technology and frequency,
- accelerator acceptance – capture, acceleration, and transport of the large muon phase space, and
- accelerator performance – issues such as potential collective effects (e.g., cumulative beam breakup) resulting from the relatively high peak current during the muon macropulse.

### 7.2.1 Muon Survival

Given their intrinsic lifetime of 2.2  $\mu\text{s}$ , one must fight muon decay during acceleration. Figure 1 shows the fractional muon survival as a function of distance along the machine for various rf real-estate gradients. An average gradient of 5 MV/m ensures >80% of the initial beam survives for injection into the storage ring.



### 7.2.2 Selection of Acceleration Technology

Muon survival demands either a high-gradient linac or high-gradient recirculating linac. The large acceptances (longitudinal and transverse) required as a product of muon cooling, combined with the fact that the source beam is bunched at 200 MHz, lead to the choice of 200 MHz rf for the first part of the accelerating system and to possibly higher-harmonic rf frequencies at higher beam energies. Several technology choices are available; they are summarized as follows:

- Straight and/or recirculating linacs, or a combination of both;
- Pulsed and/or cw rf:
  1. “fast” – on microsecond time scales, with high peak power and short pulses, or
  2. “slow” – on millisecond time scales, filling cavities slowly between pulses and accelerating the beam using the stored energy.

The desire to keep wall losses low and rf-power requirements manageable excludes recirculation and “slow-pulse” scenarios with copper linacs. Gradients achievable with conventional cw rf are too low for adequate muon survival. “Fast-fill” pulsed (conventional or srf) systems involve prohibitively high peak power ( $\sim 0.8 \text{ A} \times 50 \text{ GeV} = 40 \text{ GW}$  in each quarter of the macropulse) with associated high cost. The scenario of choice is therefore “slow-fill” pulsed or cw srf, with either straight or recirculated transport, the

idea being to fill at 15 Hz while the beam is off and accelerate using only a small fraction of the stored energy.

Recirculation saves money over a single linac. Cost considerations favor multiple passes per stage, but practical experience commissioning and operating recirculating linacs dictates prudence. Experience with recirculating linacs at Jefferson Lab suggests that recirculation should be possible once the muon energy is larger than 3 GeV. Given the large initial emittance and energy spread, a ratio of final-to-injected energy well below 10-to-1 is deemed prudent [1]. We therefore propose a machine architecture featuring a 0.2-to-3 GeV straight “preaccelerator” linac, a 3-to-11 GeV recirculating “compressor” linac (RLA1), and a 11-to-50 GeV recirculating “primary” linac (RLA2). The *preaccelerator* captures the large phase space coming from the cooling channel and accelerates it to relativistic energies. At this point, the increased muon lifetime ( $\gamma\tau$ ) allows use of a *compressor* (RLA1). During compression, the longitudinal and transverse phase spaces are shaped (while further raising the energy) for injection into the high-energy *primary* (RLA2), which then generates the 50 GeV injection energy for the storage ring.

The 200 MHz microbunch spacing from the cooling channel imposes an rf-frequency requirement of 200 MHz or one of its harmonics. The frequency of choice for both the preaccelerator and the compressor is 200 MHz, as it provides large physical apertures (well in excess of the spot sizes given in Table 2) and adequate transverse and longitudinal acceptances for the source beam. It also provides adequate stored energy to accelerate multiple passes of a single-pulse bunch train without need to refill the extracted energy between turns. Thus, the “slow-fill” pulsed scenario is viable.

The choice is less obvious for the primary (RLA2), inasmuch as the phase space is smaller and rather more manageable. Preliminary studies suggest that the first harmonic, 400 MHz, may provide an adequate aperture and acceptance. If so, the higher frequency is desirable in that it provides significant cost savings during operation (compare chapter 10). Detailed calculations affirm that the larger stored energy at 200 MHz (in contrast to 400 MHz, where the stored energy per unit length is 4 times smaller) and the longer rf wavelength generate a smaller momentum spread through the acceleration cycle. This is due to the smaller ratio of bunch length to wavelength, as well as smaller gradient sag during energy extraction over the macropulse. Accordingly, the acceptance requirement is relaxed. However, it is not clear that 200 MHz is necessary. The following “solution in progress” attempts to provide adequate recirculator acceptance to manage the larger momentum spread (and tighter bunch-length tolerances) associated with 400 MHz. Preliminary results suggest the required performance can be met. Because of significant cost savings, it is therefore our baseline frequency for RLA2. If further studies indicate that 400 MHz will not provide an adequate performance, the 200 MHz solution used in the preaccelerator and compressor will be used for the primary as well.

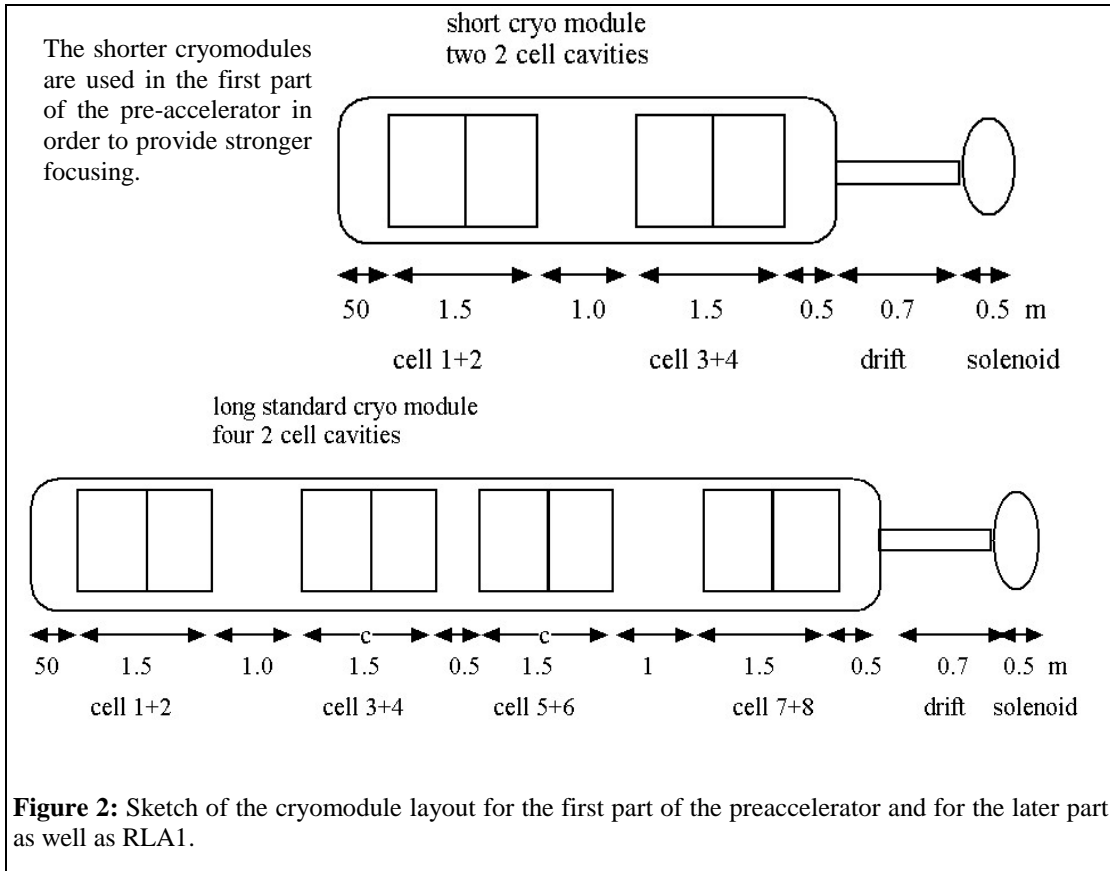
### 7.3 Machine Architecture

The proposed machine architecture is based on the aforementioned chain of three accelerators. The preaccelerator brings the beam to relativistic energies where recirculation can be invoked. The compressor (RLA1) then conditions the phase space by raising the beam energy and adiabatically damping the geometric emittance, relative momentum spread, and bunch length, so as to render the phase space volume manageable for the primary (RLA2). The principal beam dynamics issues are:

- capturing the large longitudinal and transverse emittances of the injected beam;
- minimizing the recirculatable energy;
- devising acceleration/longitudinal matching scenarios in the compressor to optimize the phase space for subsequent acceleration to full energy;
- designing RLAs 1 and 2, to include: initial and final energies, numbers of passes, and transport optics for adequate acceptance in the presence of the required longitudinal manipulations; and
- potential instabilities (such as beam breakup) at the relatively high (amp-level) peak currents present in the macropulses.

An “existence proof” with sufficient (though perhaps better than necessary) performance to address these issues has evolved based on the machine concept described above. The large injected phase space is a

primary concern, and a longitudinal capture and acceleration scenario was developed first during the design process [1]. This indicated that a 200 MHz, 3 GeV preaccelerator would provide adequate capture and a high enough energy to guarantee longitudinal matching into RLA1. A 3-to-11 GeV RLA1 concept based on 4 recirculations with 200 MHz rf was then developed. The energy range and pass number were chosen to be prudently conservative from a geometric and beam-dynamics point of view, given the need to accommodate beam splitting, recirculation, and recombination of the large phase space on multiple passes while providing adequate opportunity for longitudinal matching. The acceleration phases and momentum compactions were selected to compress both the relative momentum spread and bunch length. A notional view of the cryomodule layouts appears in Figure 2. A similar process was applied to RLA2, resulting in 5-pass primary acceleration from 11 to 50 GeV. As mentioned before, preliminary results suggest that a 400 MHz system provides adequate performance for RLA2, though with larger intermediate momentum spreads than in a 200 MHz system.



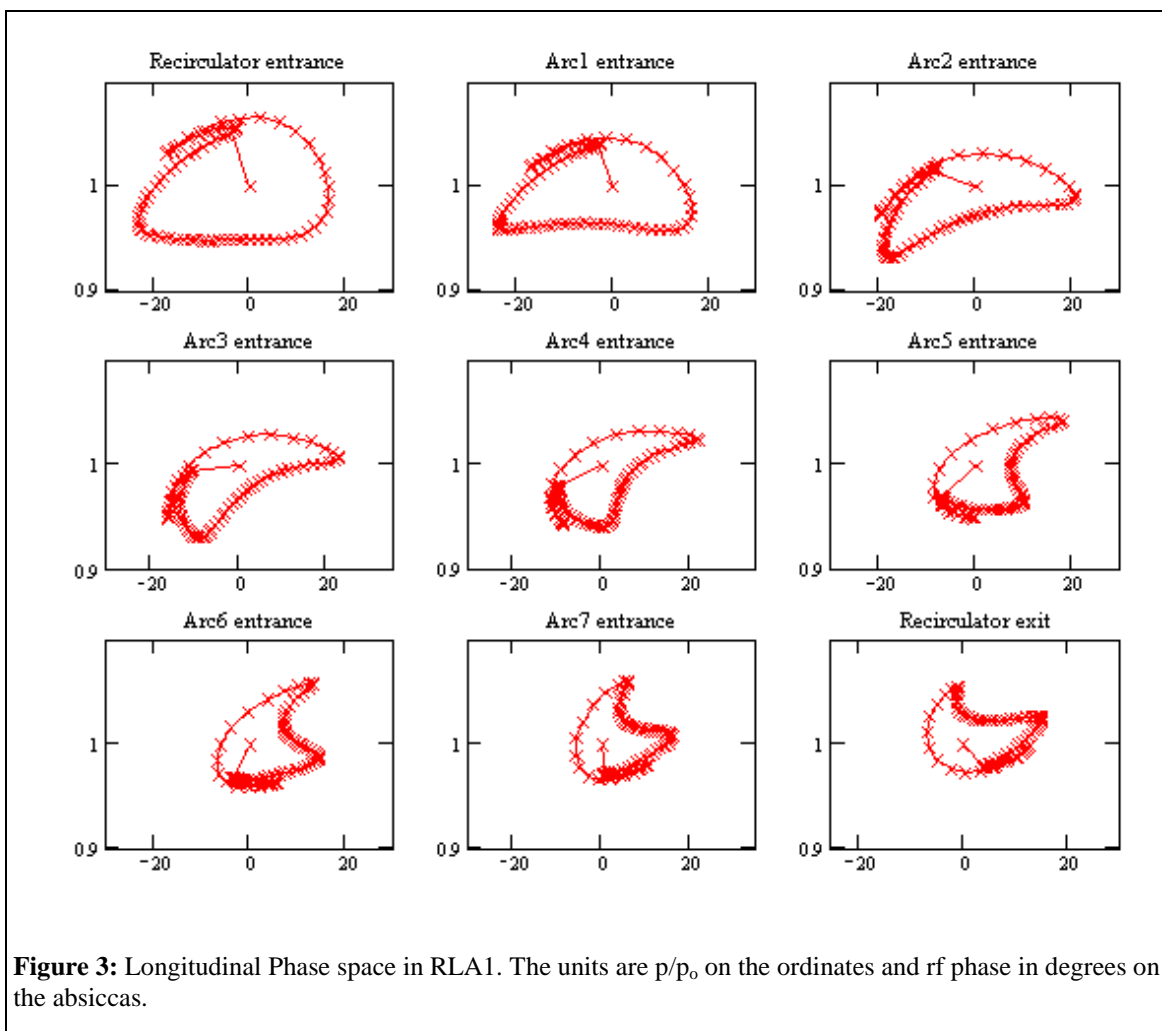
For the tracking studies an initial distribution function is generated using the following procedure. First, for each particle six random numbers, ( $j$  is the particle number, and  $i = 1, \dots, 6$ ), are used to generate an initial particle position in the 6D-phase space. The random number generator generates numbers with a Gaussian distribution, which has a mean value equal to zero and a standard deviation equal to one. Second, for each particle its radius (distance from the coordinate system center),

$$r_j = \sqrt{\sum_{i=1}^6 u_i^2}$$

is computed, and all particles for which the radius is more than 2.5 are discarded. Third, real particle coordinates are computed using following formulas:

$$\begin{bmatrix} x_\beta \\ x'_\beta \\ y_\beta \\ y'_\beta \\ s \\ \Delta p/p \end{bmatrix}_i = \begin{bmatrix} \sqrt{\varepsilon_x \beta_x} & 0 & 0 & 0 & 0 & D_x \sigma_p \\ -\alpha_x \sqrt{\frac{\varepsilon_x}{\beta_x}} & \sqrt{\frac{\varepsilon_x}{\beta_x}} & 0 & 0 & 0 & D'_x \sigma_p \\ 0 & 0 & \sqrt{\varepsilon_y \beta_y} & 0 & 0 & D_y \sigma_p \\ 0 & 0 & -\alpha_y \sqrt{\frac{\varepsilon_y}{\beta_y}} & \sqrt{\frac{\varepsilon_y}{\beta_y}} & 0 & D'_y \sigma_p \\ 0 & 0 & 0 & 0 & \sigma_s & 0 \\ 0 & 0 & 0 & 0 & \alpha_s \sigma_p & -\sigma_p \sqrt{1-\alpha_s^2} \end{bmatrix} \begin{bmatrix} u_1 \\ u_2 \\ u_3 \\ u_4 \\ u_5 \\ u_6 \end{bmatrix}_j$$

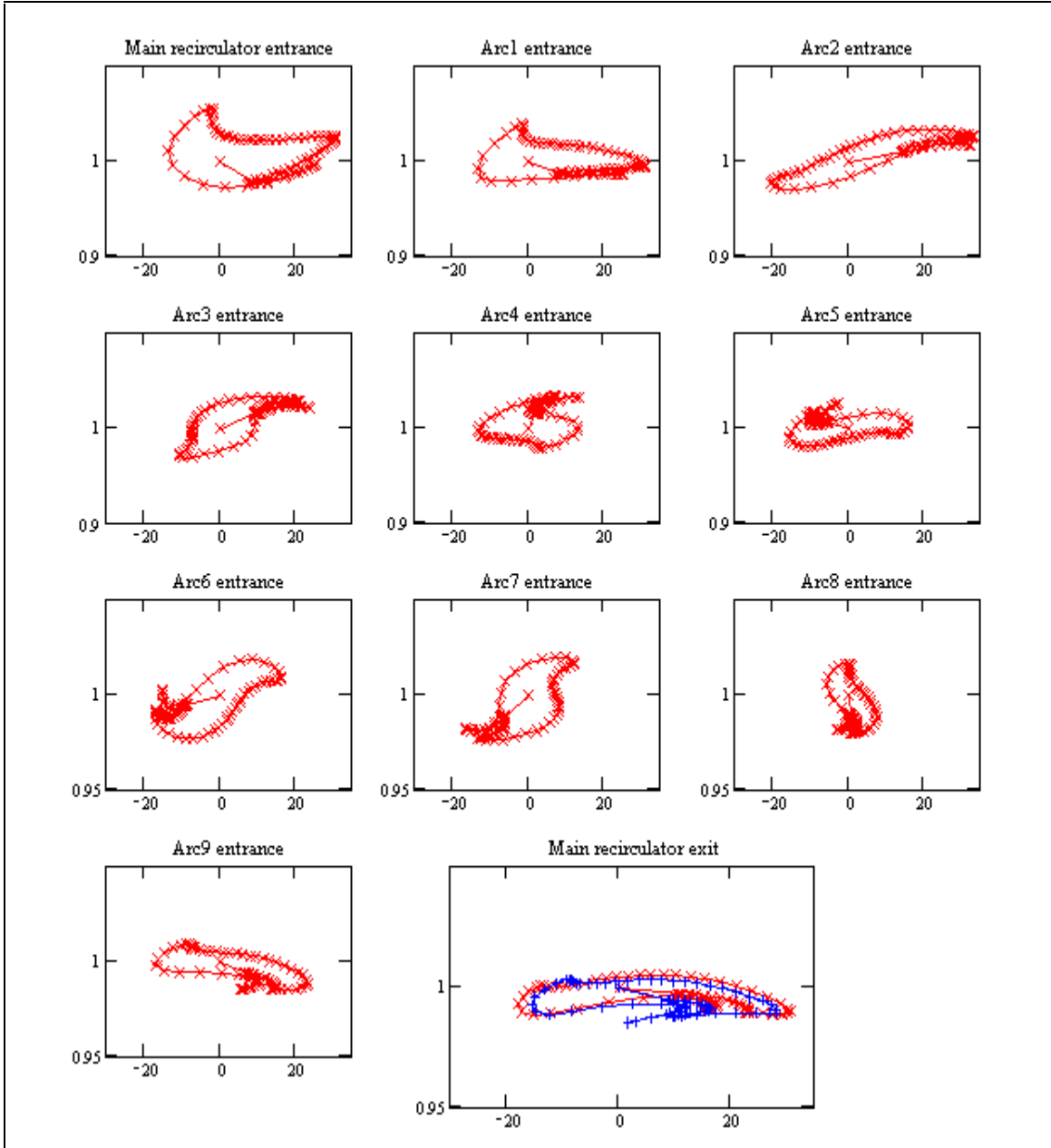
where  $\varepsilon_x$  and  $\varepsilon_y$  are the transverse rms beam emittances,  $\beta_x$ ,  $\beta_y$ ,  $\alpha_x$  and  $\alpha_y$ , are the initial beta-functions and their negative half-derivatives,  $\sigma_s$  is the rms bunch length,  $\sigma_p$  is the relative rms energy spread, and  $\alpha_s$  characterizes the rotation of the ellipse in the longitudinal phase space so that the longitudinal emittance is  $\sigma_s \sigma_p \sqrt{1-\alpha_s^2}$ . At entrance of the linear preaccelerator the following parameters have been chosen:  $\beta_x = \beta_y = 8.03$  m,  $\alpha_x = \alpha_y = -0.122$ ,  $\sigma_s = 12.11$  cm,  $\sigma_p = 0.11$ ,  $\sigma_p = -0.139$ ,  $D_x = D_y = 0$ ,  $D'_x = D'_y = 0$ . The particle ellipse in the longitudinal phase space is slightly tilted. Its axes will be coinciding with the coordinate frame axes after 0.65 m drift.



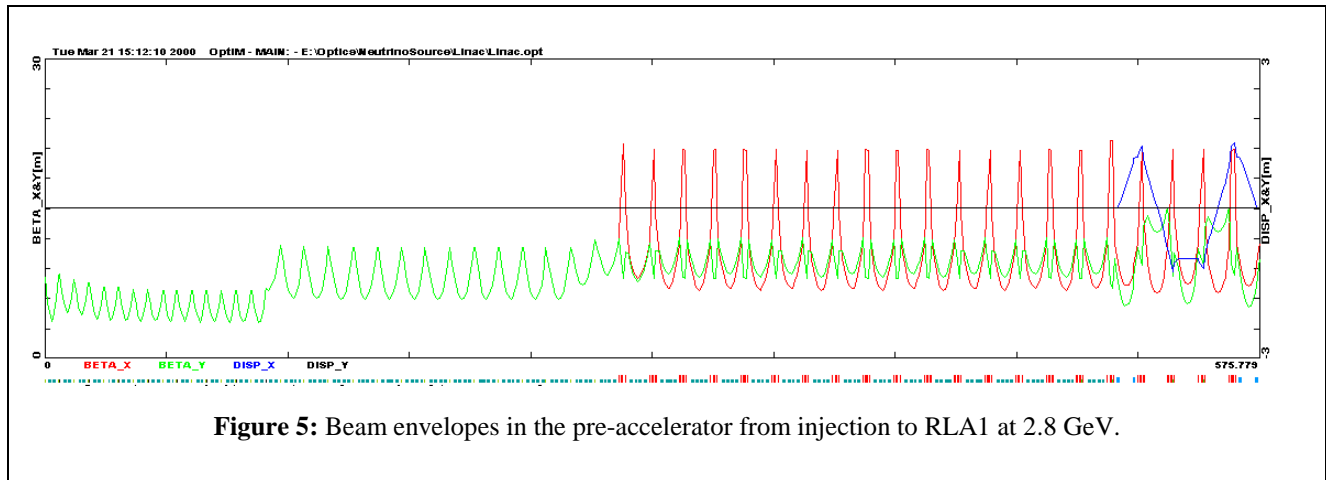
**Figure 3:** Longitudinal Phase space in RLA1. The units are  $p/p_0$  on the ordinates and rf phase in degrees on the abscissas.

Figure 3 and 4 illustrate the behavior of the longitudinal phase space through such a system; required acceleration phases and momentum compactions are shown in Table 3. Simulations of the 400 MHz scenario are at present incomplete, but they suggest that the higher frequency is feasible. A 200 MHz alternative has been studied in some detail [2] as well; it meets performance requirements and will be more robust, though at a higher initial investment and operational cost, and therefore the baseline frequency for RLA2 is taken to be 400 MHz.

Given a viable longitudinal scenario, a complete system solution was developed. The preaccelerator uses solenoid focusing between cryomodules. Beam envelopes are as shown in Figure 5. The compressor, RLA1, is a 4-pass machine comprising two 1.227 GeV linacs, with each pass split horizontally and



**Figure 4:** Longitudinal phase space in RLA2. The units are  $p/p_0$  on the ordinates and rf phase in degrees on the abscissas.



**Figure 5:** Beam envelopes in the pre-accelerator from injection to RLA1 at 2.8 GeV.

recombined using cascaded dipoles. Once separated, the individual beams are recirculated by periodic “bend-triplet-bend” arcs, producing typical beam envelopes as shown in Figure 6. Chromatic behavior is adequate to accept >10% momentum spread; no sextupole correction appears necessary.

<b>Preaccelerator</b>				
200 MHz, 0.2→ 3 GeV energy; 15 MV/m gradient, accelerating phase $-60^\circ \rightarrow 0^\circ$				
<b>RLA1 (Compressor)</b>				
200 MHz, 0.2→ 11 GeV energy; 15 MV/m gradient; total voltage/linac: 1.227 GV;				
	Kinetic energy (GeV)	$M_{56}$ (m)	Gang Phase (deg)	Total energy spread $2\Delta p/p$ %
Entrance	2.89		6	11.7
Arc 1	4.11	0.6	-22	9.0
Arc 2	5.25	0.6	-25	9.9
Arc 3	6.36	0.6	-29	9.8
Arc 4	7.43	0.6	-38	9.2
Arc 5	8.40	0.5	-45	9.6
Arc 6	9.26	0.5	-45	9.9
Arc 7	10.13	0.5	-45	9.5
Exit	11.00	0.5		8.2
<b>RLA2 (Primary)</b>				
400 MHz, 11→ 50 GeV; 15 MV/m gradient; total voltage/linac: 4.25 GV				
	Kinetic energy (GeV)	$M_{56}$ (m)	Gang Phase (deg)	Total energy spread $2\Delta p/p$ %
Entrance	11.00	2.00	-7	8.2
Arc 1	15.22	2.00	-30	6.3
Arc 2	18.9	2.00	-17	6.3
Arc 3	22.96	2.00	-30	6.4
Arc 4	26.64	2.00	-30	5.4
Arc 5	30.32	2.00	-30	4.5
Arc 6	34.00	2.00	-30	4.1
Arc 7	3.68	2.60	-11	4.3
Arc 8	41.85	2.60	-16	3.7
Arc 9	45.94	2.60	-17	2.5
Exit	50.00			1.6

**Table 3:** Accelerator Parameters.

A similar approach was adopted for RLA2, a 5-pass machine. Cascaded dipoles (Figure 7) split the passes horizontally, bringing all beamlines parallel in a few tens of meters. Because the linacs are much longer than in RLA1, additional matching is provided following the beam separation: in each pass an array of quadrupoles provides matching of the pass-to-pass beam envelopes to the regular, horizontally separated FODO arcs. Again, because the focusing is modest and the structure regular, there is no obvious requirement for chromatic correction.

The machine footprint is presented in Figure 8. For clarity and ease of comparison, the segments (preaccelerator, RLA1, and RLA2) are all positioned sequentially. For actual construction, economy suggests a more compact layout, possibly with shared usage of tunnel and conventional facilities by multiple machine segments.

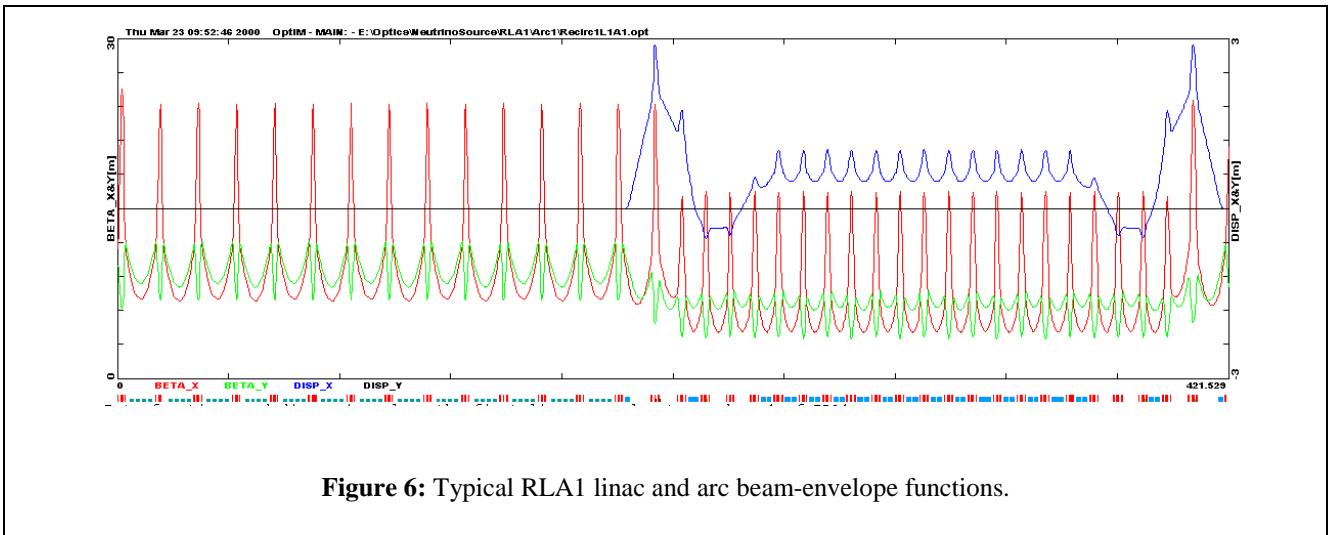


Figure 6: Typical RLA1 linac and arc beam-envelope functions.

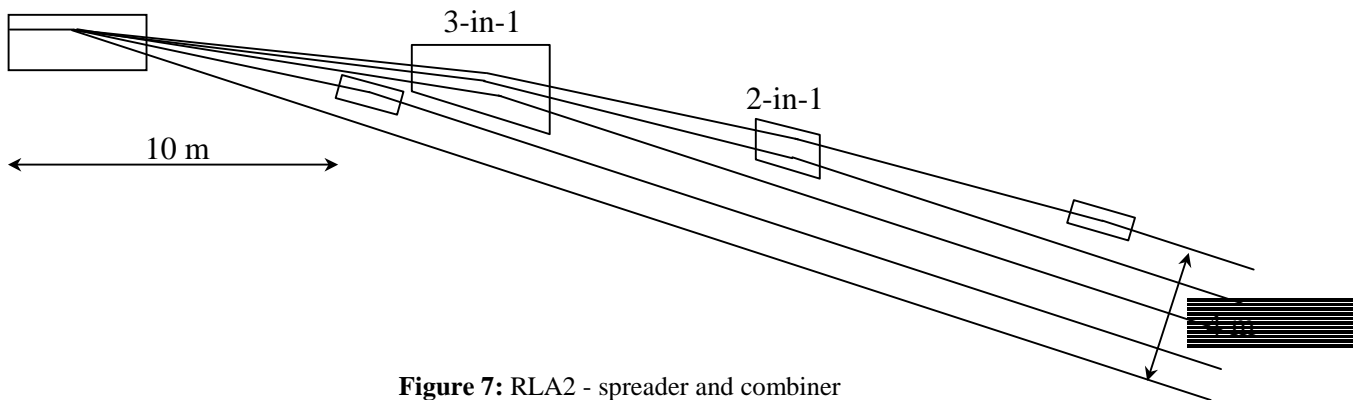
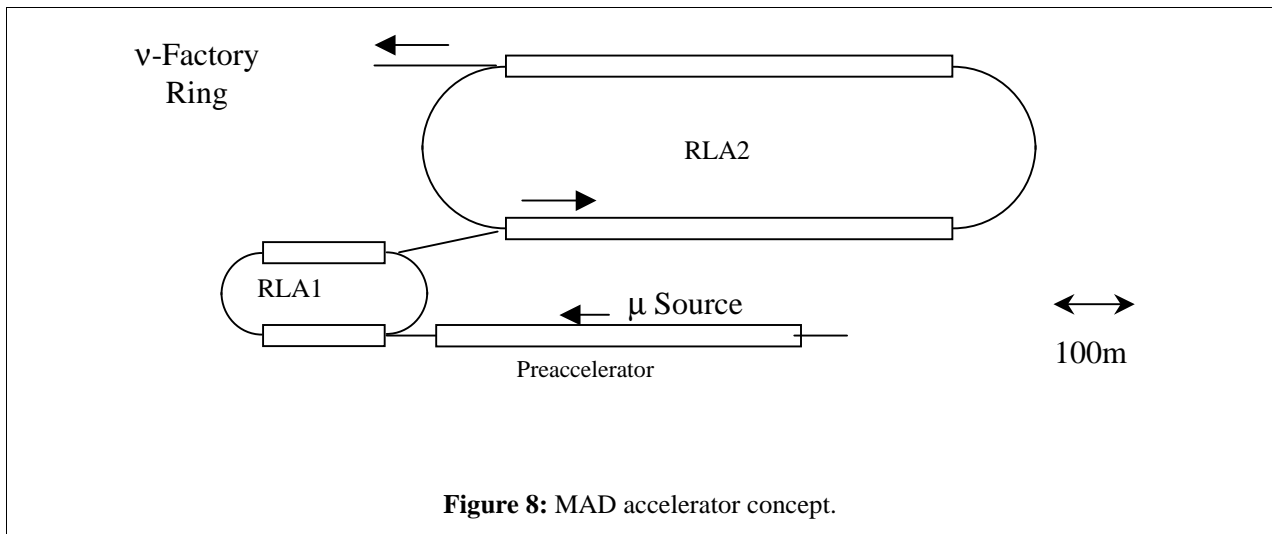


Figure 7: RLA2 - spreader and combiner



## 7.4 Collective Effects

We examine two types of beam breakup (BBU) instabilities relevant to linacs, multipass BBU and cumulative BBU [4]. Multipass BBU is of most concern in accelerators in which the beam passes many times through the same linac structure. The important mechanism causing the instability is the fact that the recirculated beam can be displaced at a given cavity due to a kick it receives from a higher-order mode (HOM) in the same cavity on a previous pass. The displaced beam can then interact with the HOM fields on subsequent passes and feed energy into it, causing subsequent bunches to be kicked even harder. There is, therefore, a closed feedback loop between the beam and the HOMs formed within the structure. The  $M_{12}$  and  $M_{34}$  matrix elements (for the recirculation) are important for the feedback of the instability.

Cumulative beam breakup, on the other hand, results from the beam interacting with two or more cavities that make up the linac. Cumulative BBU begins when a bunch receives a transverse kick from a cavity HOM resulting in a transverse displacement in a downstream cavity. The displaced bunches can drive the HOM at the second cavity coherently thereby transferring kinetic energy into the HOM. Following bunches arriving at the downstream cavity are then more strongly deflected because of the additional energy contained in the HOM.

The important difference between cumulative and multipass beam breakup is that in cumulative beam breakup there is no feedback of the HOM energy of the driven cavity back to the cavity that initially deflects the beam. The cavities act to amplify the beam offsets due to the kick, and this amplification depends strongly on the beam current. The threshold current for cumulative BBU is the current where the offsets are amplified to the point where the beam hits the beam pipe.

The threshold current for multipass beam breakup (BBU) in CEBAF had been calculated to be  $\sim 20$  mA for external  $Q$ 's of the higher-order modes (HOMs) less than  $10^5$ . Extensive simulations with TDBBU (a BBU code specially configured for recirculating linacs) seem to indicate that the threshold current scales approximately as the square-root of the product of the injection and final energies [4]. The muon linacs will require roughly an order of magnitude more cavities than the CEBAF linac; therefore, the impedance will be higher by an order of magnitude. Scaling with the rf frequency has been shown to be inversely proportional to the square of the frequency provided the accelerating gradient is frequency-independent, but it is inversely proportional to the frequency if the gradient varies linearly with frequency. Assuming the more pessimistic  $1/\omega$  scaling, and given  $E_{in}=3$  GeV,  $E_{fin}=50$  GeV for the muon linac and  $E_{in}=45$  MeV and  $E_{fin}=4$  GeV for CEBAF, we arrive at

$$I_{th} = 20mA \times \frac{1}{10} \times \frac{\sqrt{3GeV \times 50GeV}}{\sqrt{45MeV \times 4GeV}} \times \frac{1500}{200} \approx 433mA.$$

Note that if this were a truly cw linac, the average operating current would be ~50 mA, an order of magnitude lower than the threshold current. The damping time of the HOMs is  $2Q/\omega = 16 \mu\text{s}$  for  $Q=10^4$  and  $\omega=2\pi(200 \text{ MHz})$ . Therefore, during the  $10 \mu\text{s}$  between pulses, the fields will have almost decayed, implying a somewhat higher threshold for the pulsed machine than for cw.

Cumulative BBU also needs to be examined as it is typical in an S-band linac in the 100-mA range. At 200 MHz the shunt impedance and gradient scaling combined with the larger apertures should result in a factor of 10-20 higher threshold current. At ~1% duty factor, the equivalent threshold is ~100 A. In conclusion, these rough estimates based on scaling from existing accelerators indicate BBU will probably not be an issue for the muon linac if external Q's of HOMs are damped to  $10^4$  or lower. However, detailed simulations are needed to quantify more rigorously the points outlined here.

## 7.5 Superconducting RF Technology Issues

We now turn to srf considerations for a slowly pulsed, recirculating srf linac in which the macropulse acceleration is based solely on the stored energy in the cavity and not on refilling the cavities between turns or even within the macropulse. Recent technology developments suggest that one can assume the availability of superconducting cavities with single-cell properties similar to those summarized in Table 4. Here, we assume the availability of 15 MV/m gradients at both 200 and 400 MHz. The assumed unloaded quality factors ( $Q_0$ 's) are consistent with those achieved in presently available srf systems. The stored energy is given by:

$$U_{\text{stored}} = \frac{E^2 \lambda^3}{R/Q} \frac{10^4}{24\pi}$$

with  $\lambda$  the free-space wavelength,  $R/Q$  a geometric constant for the chosen cavity, and  $E$  the gradient. The data derived specifies the cw power deposited in the cryogenic system as a result of the rf power input. A summary is given in Table 5 for cw operation at 4.2 K. The number of cells is simply the installed voltage divided by the single-cell voltage in Table 4. The dynamic load is the number of cells times the power loss per cell given in Table 4.

Machine Stage	f (MHz)	$l_{\text{cell}}$ (m)	E (MV/m)	V (MV)	$U_{\text{stored/cell}}$ (J)	$Q_0$	R/Q ( $\Omega/\text{cell}$ )	$P_{\text{lost}}$ (cw, W/cell)
Pre-accelerator	200	0.75	15	11.25	1000	$6 \times 10^9$	100	209
RLA1	200	0.75	15	11.25	1000	$6 \times 10^9$	100	209
RLA2	400	0.375	15	5.625	125	$6 \times 10^9$	100	52

**Table 4:** SRF cavities for muon accelerator: single-cell properties.

Machine Stage	Installed Voltage (GeV)	#cells	CW load (kW) @ 4.2 K
Preaccelerator	3.6	320	67
RLA1	2.6	231	48
RLA2	8.5	1079	56

**Table 5:** Dynamic load, 4.2 K operation

The total cw load is ~170 kW at 4.2 K. However, the linac is to operate in pulsed mode, filling prior to injection of the macropulse and using the stored energy to accelerate the beam for multiple turns. Pulsing will significantly reduce the dynamic heat load, roughly by the rf duty cycle. Considering this operating mode, we present in Table 6 a summary of the energy extracted by the macropulse as it traverses each

accelerator segment. Table 6 gives, in particular, the energy and gradient sag due to extraction of rf energy by the beam.

Machine Stage	Charge/macropulse ( $\mu\text{C}$ )	# passes	V (MV)	$\Delta U$ (J)	$\Delta U/U_{\text{stored}}$ (%)	$\Delta V/V$ across pulse (%)
Preaccelerator	0.48	1	11.25	5.4	0.5	0.25
RLA1	0.48	4	11.25	21.6	2.2	1.1
RLA2	0.48	5	5.625	13.5	10.8	5.6

**Table 6:** Energy extraction per single cell during one macropulse.

The relative gradient sag is only half the stored-energy sag because the energy scales as the square of the gradient. The gradient sag imposes an energy slope along the macropulse, with the tail of the pulse experiencing less acceleration than the head. Given the large inherent energy spread of the beam, this sag will not be a problem in the preaccelerator or RLA1. However, it could become significant in RLA2 where the stored energy at the higher frequency is smaller and therefore more susceptible to the energy extracted by the macropulse. This might be accommodated as a part of the rf manipulations performed during longitudinal matching. For example, RLA2 arc momentum compactions and path lengths might be adjusted not only to do the required microbunch compression, but also to offset the energy slope induced across the macropulse. This possibility in principle is illustrated in Figure 3; the final frame in both Figure 3 and 4 includes data illustrating the beam-loading-induced energy slope from the head to the tail of the bunch train. The longitudinal match used to manage the large phase space similarly controls the spread across the macropulse. Once a final design is established, a methodology to implement this process operationally must be developed.

Also critical to this scenario is the availability of  $\sim 15$  MV/m gradient at 200 and 400 MHz. If the gradient were lower, the stored energy would drop quadratically, and the gradient droop would increase significantly, unless the charge per macropulse were reduced. This may ultimately motivate the use of 200 MHz rf in RLA2 with an associated increase in dynamic load but with less risk to machine performance. A detailed design study must evaluate this cost/risk/benefit tradeoff. Given, however, the availability of adequately high gradients and the development of an operationally appropriate longitudinal matching scenario both to compress the microbunch phase space and manage the gradient sag across the macropulse, the "slow-fill" scenario can be applied in this system with adequate performance. Moreover, use of 200 MHz in all machine stages (as a contingency) clearly allows this mode of operation.

Details of pulsed operation evolve from consideration of rf-power requirements. Table 7 presents power demands for each of the machine stages. The average beam-loading current is just the product of the macropulse charge ( $0.48 \mu\text{C}$ ), the repetition rate (15 Hz), and the number of passes through the segment; the average extracted power is the product of the single-cell voltage and the average beam loading current. The power to control microphonics and detuning is the product of the stored energy and the detuning bandwidth  $\delta\omega$  ( $U_{\text{stored}} \times \delta\omega$ ), here taken to be  $2\pi \times 80$  Hz. Though only an approximation, this result is valid provided the detuning bandwidth is much greater than the intrinsic bandwidth, which is certainly true for the case under consideration. This power requirement corresponds to an infinite time to fill the cavity, and therefore differs from the particular rf power demanded. Rather, at low average current the required power is determined by the necessity to establish and maintain the fields in the presence of detuning. It is therefore important to optimize the coupling by choosing the loaded Q ( $Q_L$ ) carefully.

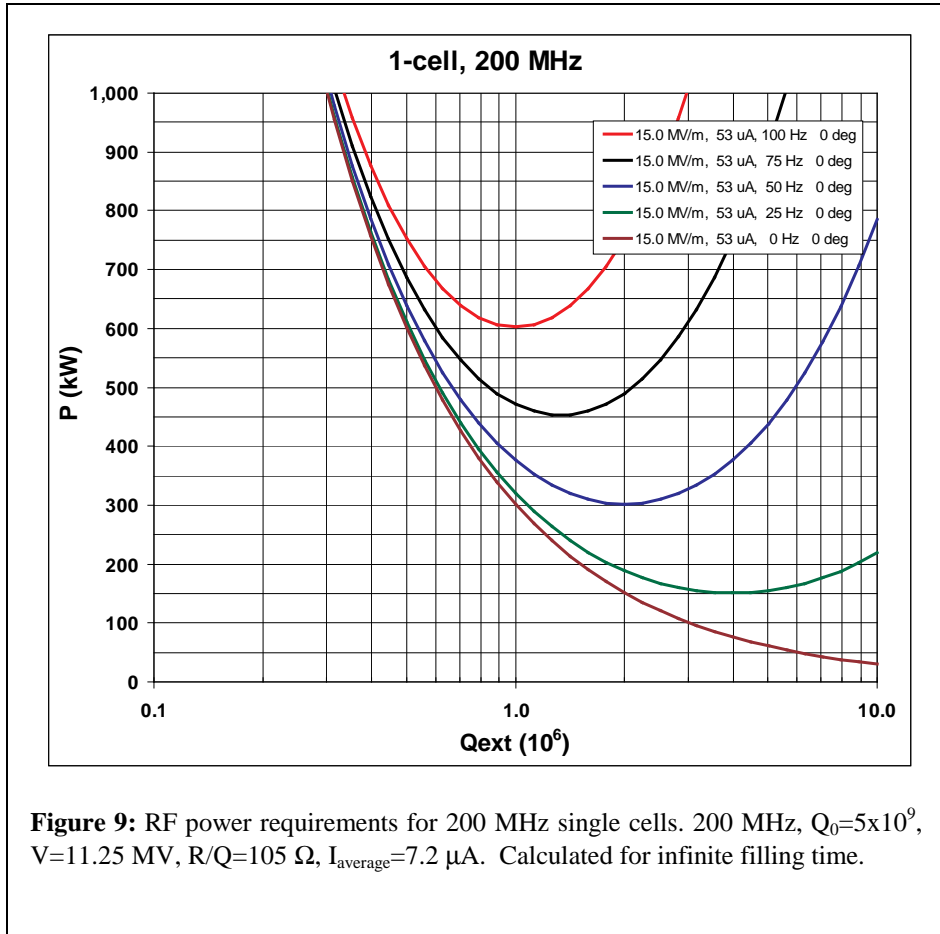
Machine Segment	# passes	$I_{\text{average}}$ ( $\mu\text{A}$ )	V (MV)	$P_{\text{average}}$ (W)	$U_{\text{stored/cell}}$ (J)	$P_{\text{control}}$ for 80 Hz bandwidth, (kW)
Preaccelerator	1	7.2	11.25	81	1000	503
RLA1	4	28.8	11.25	324	1000	503
RLA2	5	36	5.625	203	125	63

**Table 7:** Single-cell rf power requirements.

Optimization of  $Q_L$  is typically accomplished by selecting a coupling that minimizes the required rf power given the anticipated operating parameters. For infinite fill time this is straightforward. The rf power is given in terms of cavity parameters by the following expression, in which  $\Omega = \omega_0 + \delta\omega$ , with  $\omega_0$  being the cavity angular frequency and  $\delta\omega$  the angular detuning bandwidth [5]:

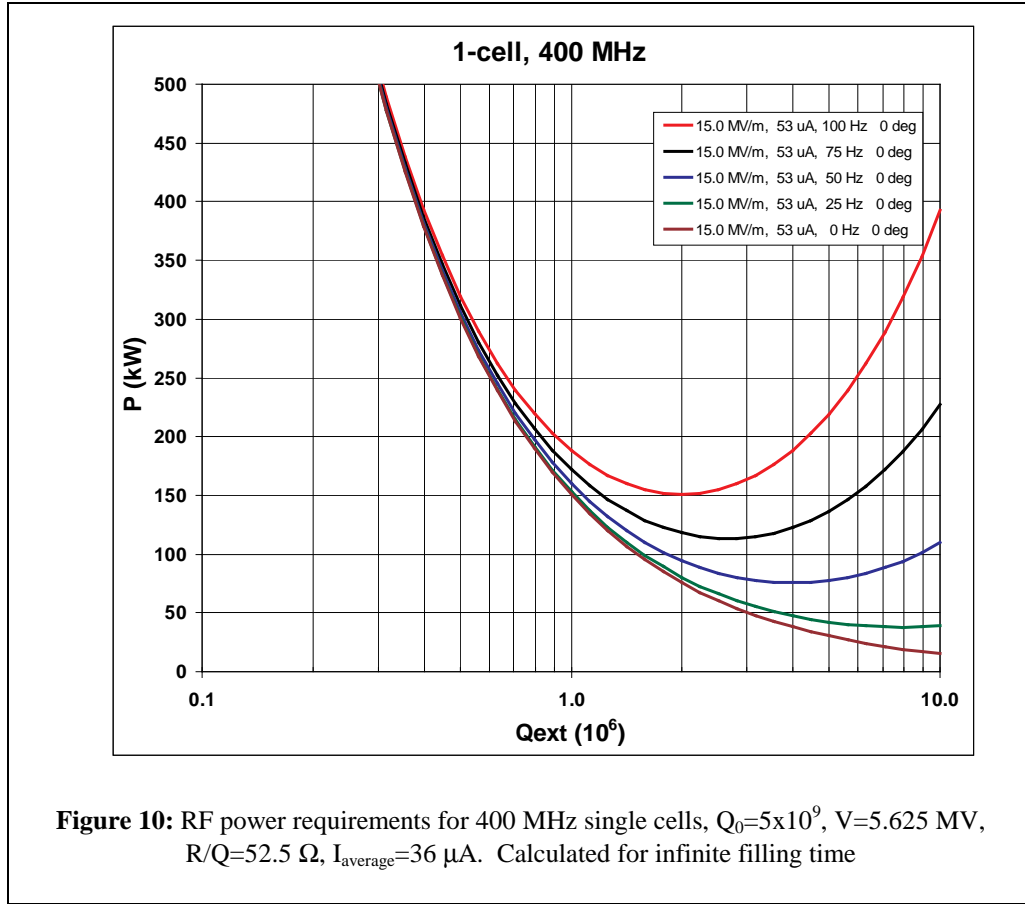
$$P = \frac{(Q_0/Q_L)^2}{4(Q_0/Q_L - 1)Q_0} \frac{V^2}{(R/Q)} \left\{ \sqrt{1 + Q_L^2 \left( \frac{\omega_0}{\Omega} - \frac{\Omega}{\omega_0} \right)^2} + \frac{(R/Q)Q_L I_{average}}{V} \right\}^2$$

Other parameters are as specified in Tables 4 through 7. Figure 9 presents the required rf power versus  $Q_L$  for several detuning bandwidths at 200 MHz for preaccelerator parameters and 400 MHz for RLA2 parameters (Figure 10). The RLA1 result will be virtually identical to that of the preaccelerator. This is because, as mentioned before, at these low average currents the required rf power is dominated by the need to establish and control the field in the presence of static and dynamic detuning, and not by the beam loading. The optimum  $Q_L$  is simply the value providing the minimum required power; it can be either read off Figure 9 or Figure 10 or derived analytically by minimizing the above power expression with respect to  $Q_L$  for the desired parameter set.



The preaccelerator (and by implication RLA1) system will handle ~80 Hz detuning with under 500 kW power provided coupling is chosen such that  $Q_L \sim 1.25 \times 10^6$ . This rf power is within the limits of present technology and can be delivered to the cell through existing, albeit state-of-the-art, couplers. Similarly, the RLA2 system will manage ~80 Hz detuning with ~125 kW power when the coupling is chosen so that

$Q_L \sim 2.5 \times 10^6$ . The power requirements are similar to the estimates given above; they are very preliminary. They are again based on the assumption that the system operates with very small currents and even more on the fact that a detuning bandwidth of 80 Hz is feasible. Especially the second part can only be answered by an R&D program, which would emphasize this question by constructing a cavity especially suited for this purpose (i.e., minimizing Lorentz-force detuning and microphonics).



For finite filling times, the analysis is less transparent. In this case (in the zero-current limit applicable to this machine), the power as a function of fill time  $T$ , coupling  $\beta=Q_0/Q_L-1$ , stored energy  $U$ , detuning bandwidth  $\delta\omega$ , and intrinsic bandwidth  $\Delta\omega_0=\omega_0/Q_0$  can be derived from

$$P = \frac{U \Delta\omega_0}{\left[1 - \exp\left(-\frac{T\Delta\omega_0(\beta+1)}{2}\right)\right]^2} \frac{1}{4\beta} \left[ (\beta+1)^2 + \left(\frac{2\delta\omega}{\Delta\omega_0}\right)^2 \right]$$

The optimum  $Q_L$  (or coupling  $\beta$ ) is that which minimizes the required power. This case is not amenable to simple analytic treatment because of the time dependence. Instead, a numerical solution is used to minimize the power as a function of coupling. Figure 11 presents the optimum power, coupling, and detuning as functions of fill time (fill time  $\equiv$  rf pulse length in this case) for parameter sets appropriate to this machine. The asymptotic limit is simply that given above; as the fill time decreases to below  $\sim 10$  ms, the required power rises, and the optimum coupling and bandwidth change.

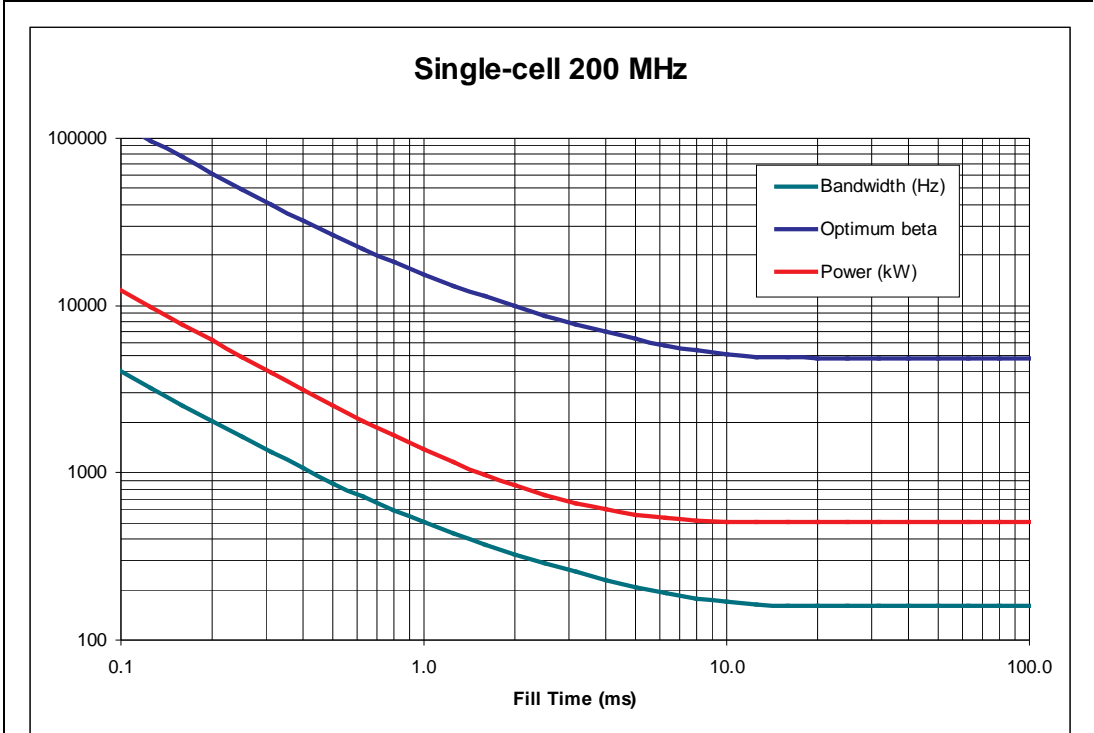


**Figure 11:** Optimized power, coupling, and bandwidth as a function of fill time. (200 MHz system case).

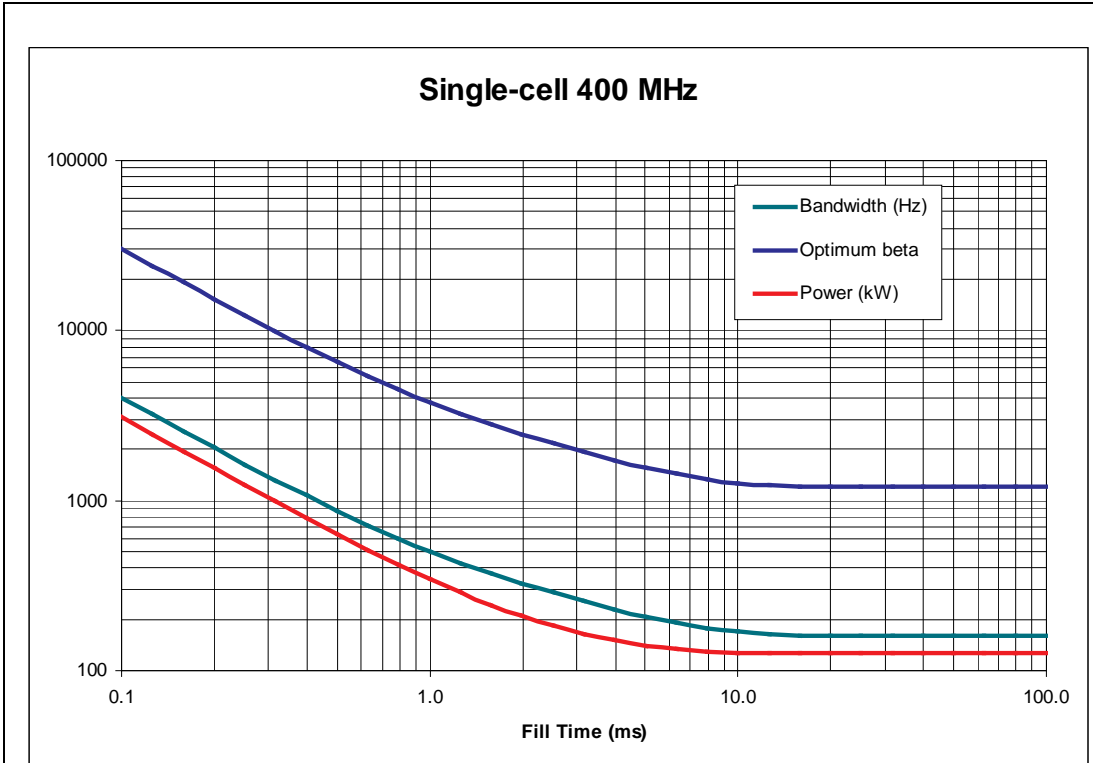


**Figure 12:** Optimized power, coupling, and bandwidth as a function of fill time. (400 MHz system case)

For a more detailed design a filling time (or duty cycle) must be chosen consistent not only with rf power requirements, but also with the constraint of cryogenic loads in place. For this study, we examine a fill time of 2 ms, which corresponds to a duty cycle of 3% at 15 Hz macropulse repetition rate. The preaccelerator and RLA1 will optimally require 820 kW at a coupling of about 9750, corresponding to a  $Q_L$  of  $6.1 \times 10^5$ , while RLA2 will require 200 kW at a coupling of 2500, and a  $Q_L$  of  $2 \times 10^6$ . At this duty cycle, the dynamic heat load for the full machine is 3% of the 171 kW cw load quoted in Table 5, or 5 kW. Given the details of a full design, this type of analysis should be done to establish the cost optimum of the rf drive and cryogenic systems.

The use of modestly long (2 ms) rf pulses and relying on the stored energy in the cavity to accelerate the beam thus allows use of almost available (not quite state-of-the-art) couplers, with an associated small dynamic cryogenic load of 5 kW. The required rf power is specified not by the beam but rather by the control system (to manage static and dynamic detuning) as well as filling the volume of the cavity with enough energy to establish the gradient. The primary issues for this scenario are the availability of sufficiently high gradients (to provide adequate stored energy) and proper specification of the cavity external Q (to optimize rf power and duty-cycle/cryogenic requirements). The rf systems which are anticipated for the accelerator are described in Chapter 10.

We note that alternative scenarios are possible. The above discussion details a system in which the beam is accelerated entirely by energy “slowly” stored in srf cavities between macropulses. Earlier discussions have noted that directly driving the beam with rf power (“fast”-pulse scenarios) during the macropulse requires prohibitively large peak power. We have not, however, determined the system-wide optimum fill time. It may be possible, for example, to reduce beam-loading-induced momentum spread across the macropulse by adopting a fill time that replenishes the stored energy between individual *turns* of the macropulse [7]. Though requiring more peak power than refilling between macropulses, this scheme does not require the peak power demanded by “fast”-pulse scenarios such as those used in copper linacs. In addition, it provides better momentum spread through the acceleration cycle and allows use of a lower rf duty cycle. It may also reduce the required average rf power and thereby provide (through reduced transport and cryogenic demands) lower costs. A detailed system design must incorporate a cost/performance optimization between peak-power and average-power demands, momentum-spread-driven transport-system requirements, and dynamic heat load/cryogenic-system loads.

## 7.6 Conclusions

A first, but preliminary, design concept for the muon accelerator has been devised. Based on the analyses presented here, it seems feasible in that it meets the performance requirements. Nonetheless, acceleration of a large-emittance muon beam is clearly challenging. Moreover, the need to achieve high energy makes this system a cost driver. SRF technology minimizes the total cost because it circumvents development of rf-power sources that would be needed for normal-conducting technology, which would be, even if they already existed, the major part of the cost. An unconventional way of using the large stored energy in a low-frequency, high-gradient srf cavity has been delineated. Acceleration based solely on the stored energy in the cavity allows filling the cavity extremely slowly which reduces peak-power demands. On the other hand, a very small detuning bandwidth, driven by microphonics, is required, which will not be easy to achieve in large cavities.

## REFERENCES

- [1] For a discussion of linac dynamic range (injected-to-final energy ratio) see, *e.g.* D. Douglas, “Lattice Design Principles for a Recirculated, High Energy, SRF Electron Accelerator”, Proceedings of the 1993 Particle Accelerator Conference, IEEE Catalog No. 93CH3279-7, p. 584 (1993).
- [1] Various similar solutions were independently developed by D. Neuffer, S. Berg, and V. Lebedev; the latter is presented here and is documented on the Web at <http://www.jlab.org/~lebedev>.

- [2] V. Lebedev, *op. cit.*
- [3] This section was kindly provided by L. Merminga.
- [4] J. J. Bisognano, private communication.
- [5] G. A. Krafft, S. N. Simrock, and K. L. Mahoney, "Beam Loading Studies at CEBAF", Proceedings of the 1990 Linear Accelerator Conference, LANL Report LA-12004-C, p. 300 (1990).
- [6] G. A. Krafft, JLAB-TN (in preparation)

